ROYAL SOCIETY
OF CHEMISTRY

PAPER

Check for updates

Waste mediated synthesis of iron nanoparticles using *Aegle marmelos* peel extract for catalytic degradation of toxic dye contaminants†

Anju Srivastava, Sriparna Dutta and Reena Jain [ID] *

The present work sheds light on the benign synthesis of iron nanoparticles from aqueous plant extract derived from waste peels of *Aegle marmelos* for catalytic degradation of two commercial toxic dyes-Eosin Yellow (EY) and Fuchsin Basic (FB).

Sustainability spotlight

Today, it is widely recognized that green chemistry (GC) is the key tool to achieve sustainability. With only a very few years left to accomplish the seventeen Sustainable Development Goals (SDGs), outlined by the various member countries of U.N. in the 2030 Agenda that unified the world towards working together to render a safer and cleaner planet, the significance of the adoption of green chemistry has acquired even more prominence. Fortunately, GC has provided highly promising solutions, including the introduction of a circular economy for combating several global waste related environmental and societal challenges on the horizon. Indeed, it offers prospects of solving the twin problems of resources and waste by making the latter the solution to the former. Amongst a diverse variety of waste materials, plant wastes/food wastes have been utilized proficiently for the synthesis of a broad spectrum of valuable products including nanoparticles that continue to spread a radical revolution in a myriad of applications including catalysis, water remediation, drug delivery, *etc.* with their remarkable properties at the nanoscale. In fact, the waste mediated synthesis of nanoparticles implementing the green chemistry principles has drawn the attention of researchers as they offer a sustainable and appealing approach compared to the conventional chemical reductant based methods that rely on the use of toxic precursors and also generate a large amount of waste. In this endeavor, through the present work, we have divulged a sustainable method for synthesizing iron nanoparticles from aqueous plant extract derived from waste peels of *Aegle marmelos* and $FeCl_2$-the iron precursor and their application as a catalytic material for the degradation of two commercial dyes-Eosin Yellow (EY) and Fuchsin Basic (FB) that have been degraded readily showing a removal efficacy of more than 95% at 318 K within 25 minutes, thus showing prospects for large-scale real time applicability. Due consideration has been given to the assessment of the recyclability, reusability and heterogeneity of these nanoparticles, and the results indicated that the nanoparticles are stable and iron practically does not diffuse to the solution from the core of the nanoparticles.

Introduction

Recent advancements in the area of nanoscience and nanotechnology have led to the development of efficient nanomaterials that have shown remarkable activity in diverse fields including water treatment, catalysis, soil remediation, drug delivery, *etc.* The enhanced activity as a result of size reduction is obvious in view of the increased surface area to volume ratio and notable changes in physicochemical properties at the nanolevel. Amongst a diversity of nanoparticles synthesized so far, iron-based nanoparticles have gained a lot of importance in current times owing to their riveting magnetic properties, low toxicity, abundance, and exceptional thermal and chemical stability.[1,2] In view of their significance, a number of methods *viz.* chemical, physical and photochemical have been adopted for the rapid synthesis of these nanoparticles. These traditional methods, however, involve the use of toxic reagents, hazardous

organic solvents, and non-biodegradable stabilizing agents, besides the tedious process of synthesis.[3,4] Therefore, it is imperative to design and develop alternate green synthetic strategies which pose little or no damage to human health and the environment.[5,6]

Within this context of innovative green methodologies, plant-based synthesis of nanoparticles has enthused the researchers as they offer an environmentally benign pathway that can avoid the use of toxic additives, specifically external reductants and capping agents as well as organic carcinogenic solvents.[7–11] The phytochemicals present in plants such as flavones, terpenoids, ketones, aldehydes, amides, and carboxylic acids not only serve as excellent reductants but also as stabilising agents, imparting nanoparticles with considerable stability against agglomeration and oxidation.[12,13] Rao *et al.* reported the synthesis of Fe^o/Fe_3O_4 nanoparticles using pomegranate (*Punica granatum*) leaf extract.[14] The authors delineated the role of various polyphenols in the plant, which act both as a reducing agent as well as a capping agent, resulting in the synthesis of stable nanoparticles without the addition of any external surfactant or polymer. Similar studies by Aisida *et al.* have highlighted the role of *Moringa oleifera* leaf extract as an

Hindu College, Department of Chemistry, University of Delhi, Delhi-110007, India. E-mail: reenajain_70@yahoo.co.in

excellent reducing agent for the biogenic synthesis of magnetic iron nanorods with an average particle size of 15.01 ± 6.03 nm.[15]

To further enhance the green credentials of a protocol, increasing attempts are now being directed towards utilizing waste for deriving valuable resources such as nanoparticles, and thus, the concept of a circular economy has acquired immense significance. Consequently, it is not surprising to note that a variety of agro wastes ranging from *Cocos nucifera* coir, corn cobs, fruit seeds and peels, wheat bran, rice bran, to palm oil mill effluent are being utilized to synthesize iron nanoparticles, which is certainly a more sustainable approach as it also aids in resolving the challenges associated with waste.[16] Chemically, these agro wastes offer a rich source of biomolecules and bio reductants in the synthetic process.[17–19] In a quest to accomplish a sustainable and greener strategy for obtaining iron oxide nanoparticles, Venkateswarlu *et al.* utilized the plantain peel extract.[20] The TEM analysis showcased the spherical morphology of the Fe_3O_4 nanoparticles with a particle size less than 50 nm, having good dispersibility. Working on similar lines, Prasad *et al.* showed that watermelon rind extract, which is a rich source of cellulose, pectin, citrulline, carotenoids and proteins, can function as a promising capping and reducing agent, providing magnetic Fe_3O_4 nanoparticles with good catalytic activity.[21] Very recently, Sharma *et al.* reported the synthesis of magnetic Fe_3O_4 nanoparticles using potato peel extract and demonstrated their catalytic ability in the degradation of rhodamine B dye.[22]

In the list of iron based nanoparticles synthesized so far, the contribution of nano-zero-valent-iron (nZVI) in environmental remediation has earned substantial recognition as it is not only efficient in removing heavy metals such as Cr(VI) and Pb(II) in groundwater, but also in removing common organic contaminants such as TNT, carbon tetrachloride, trichloroethene and many more.[23,24] In the past, a myriad of physical and chemical approaches, such as membrane filtration, adsorption, chemical precipitation, oxidation and electrochemical treatment technologies have been employed to remove these pollutants and make water clean.[25] However, most of these techniques are either highly expensive or less efficient.[26–28] The zero valent iron nanoparticles primarily work as a Fenton-like catalyst for the oxidative degradation of organic dyes and other organic pollutants. Literature reports clearly highlight the significance of Fenton-like oxidative catalytic processes as they have displayed great potential in eliminating organic pollutants under mild reaction conditions (non-acidic/neutral pH). Unlike the classical Fenton process which relies on the use of dissolved ferrous ions as the starting reagent, the greener methodology relies on the *in situ* generation of hydroxyl radicals upon the reaction of hydrogen peroxide with iron oxide or zero-valent iron nanoparticles. The research work by Shahwan *et al.* proves the efficiency of the iron nanoparticles derived using green tea extracts which worked as a Fenton like catalyst in the degradation of dyes.[29] A similar study by Kuang *et al.* and Wu *et al.* highlights the degradation of malachite green dye and other compounds using the iron nanoparticles derived from tea extract and also validates the Fenton-like catalytic efficiency of green synthesised iron nanoparticles.[30,31]

With the prime objectives of working towards resolving waste related challenges and also contributing towards the sixth sustainable development goal-clean water & sanitation, the present study attempts the green synthesis of iron nanoparticles using aqueous extract of waste peels of *Aegle marmelos* fruit (commonly known as bael) which is a rich source of different phytoconstituents such as alkaloids, coumarins, terpenoids, fatty acids, and amino acids.[32] The bael peel is also rich in polyphenols, which act both as a reducing agent as well as a capping agent. A range of important spectroscopic and microscopic techniques such as FT-IR SEM/EDX, TEM and XRD have been utilized for acquiring insights into the structural aspects. Furthermore, the catalytic potential of the synthesised Fe NPs as a Fenton catalyst has been investigated in the removal of an anionic dye (Eosin Yellow, EY) as well as a cationic dye (Fuchsin Basic, FB), which served as the model pollutant dyes. To delve into the mechanistic aspects, oxidative degradation, using H_2O_2, was studied over a wide range of temperatures. Due consideration has been given to the assessment of the recyclability and reusability of these nanoparticles.

Results and discussion

Insights into structural and morphological aspects

The characterization of the synthesized iron nanoparticles was performed using various instrumental techniques including FTIR, XRD, SEM, TEM and EDX. First, to ascertain the presence of functional groups, FTIR spectroscopy was performed. Fig. 1 reveals the FTIR spectrum of iron nanoparticles which displays the presence of strong intense absorbance bands appearing at 3401 cm^{-1}, 1672 cm^{-1} and 1047 cm^{-1}. The broad band centering at around 3401 cm^{-1} corresponds to the stretching vibrations of the hydroxyl group (–OH) in H-bonded polyphenols.[22] These polyphenols possess strong antioxidizing properties and thus can effectively reduce Fe(II) ions and get adsorbed on the surface of iron nanoparticles.[31] This endows the nanoparticle with a protective layer that insulates the particle from outer atmospheric conditions, thereby improving the shelf life of these particles. The surface chemical moieties that capped and reduced the iron oxide nanoparticles were affirmed by the FT-IR technique. In addition, it also confirmed the binding of chemical groups from the extract on iron oxide nanoparticles. The signals at 1672 cm^{-1} and 1405 cm^{-1} can be attributed to the –C=O and –C=C stretching vibrations, which indicates the presence of flavonoids and terpenoids in the fruit extract of *A. marmelos*.[33,44] The bands in the region 2962–
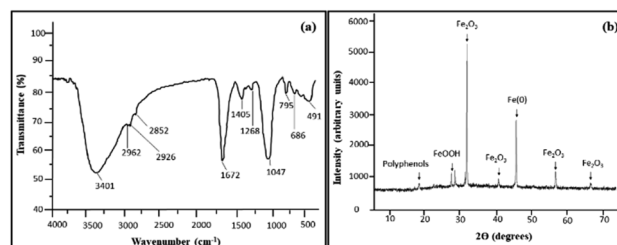

Fig. 1 (a) FT-IR spectrum and (b) X-ray diffractogram of Fe NPs.

2852 cm^{-1} are attributed to νC–H, whereas the absorbance bands at 1268 cm^{-1} and 1047 cm^{-1} can be attributed to the –C–O stretching vibrations of carboxylic acid, ester, and ether groups of the proteins and metabolites present in the extract which might be involved in the reduction process. Hence, the IR analysis indicates that these polyphenolic compounds form an integral component of iron nanoparticles by attaching themselves to the surface through the surface chemical moiety. Furthermore, the weak band around 491 cm^{-1} is assigned to Fe–O stretching vibrations, confirming the formation of Fe_2O_3 and FeO(OH) on the surface of Fe-NPs which corroborates well with the result derived from XRD analysis. Thus, IR analysis suggests that these phytochemicals are present and play a major role as bioreductants as well as stabilising agents in the synthesis of FeNPs.[30,31]

The crystalline nature of the synthesised Fe NPs from the waste peel extract of *A. marmelos* fruit was confirmed from the powder X-ray diffraction study. The X-ray diffractogram of the synthesized Fe NPs (Fig. 1(b)) revealed characteristic peaks at 2θ = 31.62°, 40.43°, 56.44°, 66.16°, which match well with the peaks displayed by the hematite (α-Fe_2O_3) phase, as evident from the JCPDS card no. 33-0664.[34] Furthermore, the peaks appearing at 2θ = 27.40° and 28.39° correspond to ferric hydroxide/ferric oxohydroxide Fe(OH)$_3$ and FeO(OH).[18] In addition, a sharp peak at 45.46° is in concordance with the zerovalent iron (α-Fe) phase. [JCPDS card no. 06-0696].[32] On the basis of an X-ray diffraction study, it was therefore confirmed that Fe NPs contain nano-zero-valent iron (nZVI) along with iron oxides and oxyhydroxide.[30,31] An additional peak at 18.36° is due to polyphenols present in the bael extract.[12] Undoubtedly, the intense and sharp peaks are suggestive of the crystalline nature of the synthesised nanoparticles which is in good agreement with the other studies.[35] The average crystallite size calculated using the most intense peak at a 2θ value ∼31.65° is ∼44 nm by applying the Debye–Scherrer formula. A similar mean particle size has also been reported by Shahwan *et al.*[29]

SEM and EDX analyses were performed in order to elucidate the morphology, surface details and elemental composition of the Fe NPs. The SEM image of Fe NPs as shown in Fig. 2(a), revealed that the nanoparticles possess spherical morphology and existed in the agglomerated form. Such agglomeration could possibly be due to the presence of biomolecules on the surface of the particles which can greatly influence the final morphology and size of these nanoparticles.[31] Also, H-bonding present in these biomolecules plays an important role in their aggregation.[36,37] The results are in agreement with the observations made by Feng *et al.* in which the iron nanoparticles have been described to exist in close contact with each other due to the high surface energy and magnetic properties.[38]

The EDX spectrum of the obtained iron nanoparticles [Fig. 2(b)] depicted the peaks corresponding to C, O, Cl and Fe. The presence of the K-α line at 6.37 keV confirmed the presence of elemental iron.[33] The two K-α lines at 0.28 keV and 0.6 keV correspond to C and O atoms, respectively. The atomic composition of individual elements was 30.91% C, 42.86% O, 25.14% Fe and 1.09% Cl. The peaks due to carbon and oxygen provide evidence in support of the fact that the organic matter derived from bael peel extract existed at the surface of nanoparticles (also shown by FT-IR analysis).[30] The appearance of a prominent peak of chlorine could be ascribed to the residual ferrous chloride salt solution that was used for the synthesis of the nanoparticles.[29]

For acquiring details pertaining to the overall morphology of the iron oxide nanoparticles, TEM analysis was also performed. As evident from Fig. 3, the TEM image of Fe NPs revealed that the nanoparticles exhibit spherical nanostructures with an average size ranging between 40 and 50 nm.

Catalytic activity of Fe NPs for dye degradation

To study the efficacy of the iron nanoparticles as a Fenton-like catalyst for oxidative degradation, an anionic dye (Eosin Yellow, EY) and a cationic dye (Fuchsin Basic, FB) were chosen as model substrates. The plots for the removal efficiency of the dye as a function of time are shown in Fig. 4. The results indicated excellent catalytic potential with a removal efficiency of 97% for EY and 95% for FB within 20 and 25 minutes, respectively, at 318 K. It is clearly evident from Fig. 4 that the removal of EY proceeds almost instantaneously, with 55% of the dye getting degraded within the first 5 minutes of the reaction in comparison to only 29.75% of FB under similar reaction conditions. A control experiment using only H_2O_2 was performed under similar reaction conditions and the removal efficiency obtained was as low as 4.8%, indicating that the dye cannot be degraded using H_2O_2 alone. These findings suggest that Fe NPs act as excellent Fenton-like catalysts.

Furthermore, the effect of pH, which is one of the most essential regulating parameters was investigated in detail using
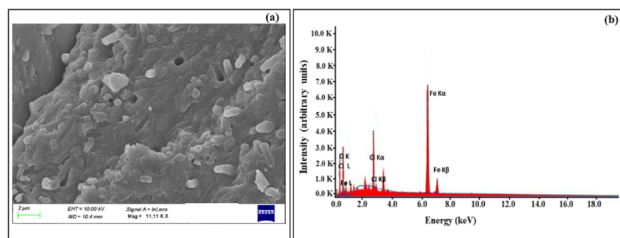

Fig. 2 (a) SEM micrograph and (b) EDX spectrum of Fe NPs.
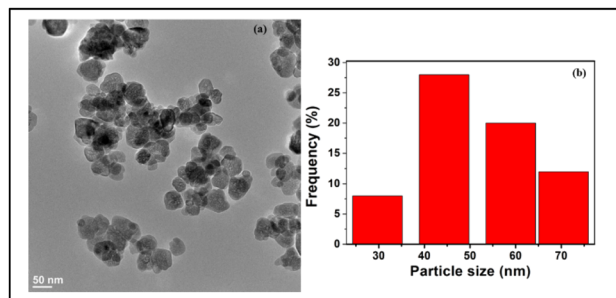

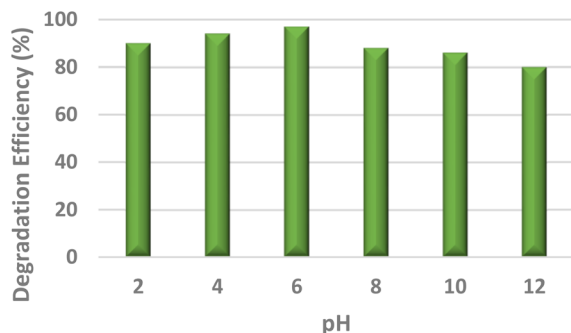**Fig. 3** (a) TEM image of Fe NPs and (b) inset: number-weighted particle size distribution (PSD).

Fig. 4 Effect of pH on degradation of Eosin Yellow dye reaction type: Fenton, reaction conditions: [45 mL of Eosin Yellow dye solution, (8 mg L^{-1}), 5.0 mL aqueous H$_2$O$_2$ (30%) solution (0.163 mol), Fe NPs (50 mg), λ_{max} = 518 nm].

the catalyst's point of zero charge. As is quite pertinent from previous literature reports, synthetic iron oxides have a point of zero charge (PZC) value lying between 7 and 9.[49] The surface of the catalyst becomes positively charged, favouring electrostatic interactions with the anionic dyes, as soon as the pH value drops below pHpzc. As per the findings of the study involving the degradation of Eosin Yellow dye in the presence of the synthesized catalyst conducted at different pH values of 2, 4, 6, 8, 10 and 12, it was observed that the best results were obtained at pH 6, showing a degradation efficiency of more than 15% than that at pH 12 (Fig. 4). As per literature findings, the OH radicals predominate at neutral or higher pH. However, at high pH values, retention of anionic dyes with the negative charge available on the catalyst's outer surface is prevented.

Various optimization studies were carried out to achieve the best conditions for the degradative processes. Consequently, the influence of temperature on the catalytic activity of Fe NPs towards the removal of dyes was examined and the outcomes are shown in Fig. 5. The experiment was conducted at four different temperatures, 298, 303, 308 and 318 K, using the same concentrations of dye and catalyst. The results indicate that for Eosin Yellow, a removal efficiency of 55%, 59%, 72% and 97% was achieved within 20 minutes at 298, 303, 308 and 318 K, respectively, while for Fuchsin Basic, removal rates of 45%, 48%, 66% and 95% were achieved in 25 minutes under similar
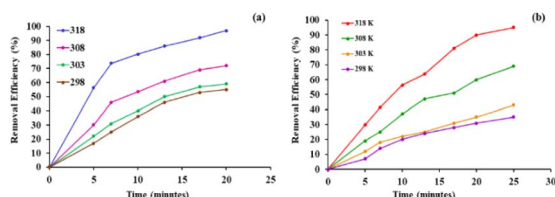
temperature conditions. These results indicated that the increase in temperature resulted in an increase in removal efficiency which could be attributed to the increased generation of hydroxyl radicals and also an increase in collision frequencies between the reactant molecules, which facilitated the degree of adsorption of the dye on the surface of nanoparticles.

As supported by the previous studies[30,39] the present oxidative degradative process followed pseudo-first order kinetics in accordance with the following equation

$$\ln \frac{C_t}{C_0} = -k_{obs}t \tag{1}$$

where k_{obs} = pseudo-first order rate constant (min^{-1}), C_0 = initial concentration of dye solution (mg L^{-1}), and C_t = concentration of dye at time t (minutes).

As shown in Fig. 6, a plot of $\ln(C_t/C_0)$ *versus* time (t) fits well with the pseudo first order kinetics and a linear relationship between $\ln(C_t/C_0)$ and reaction time is observed with high correlation coefficient R^2 values (Table 1). Studies have suggested that compounds displaying a removal efficiency greater than 15% are more likely to follow both coagulation (surface adsorption) and oxidative pathways during their degradation.[40,41]

Furthermore, for the calculation of the apparent activation energy (E_a) for the degradation of the dye, the Arrhenius equation was used.

The linear relationship obtained in a plot of $\ln k_{obs}$ *versus* $1/T$ clearly depicts the pseudo-first order model for dye degradation (Fig. S1, ESI†). The values of activation energy (E_a) for oxidative degradation of Eosin Yellow and Fuchsin Basic are calculated to be 51.05 and 59.03 kJ mol^{-1}, respectively. A similar kind of conclusion was also drawn from degradation of monochlorobenzene using iron nanoparticles in the presence of H$_2$O$_2$.[30] Also, the values were found to be greater than the activation energy of a diffusion-controlled ($\sim$29 kJ mol^{-1}) reaction.[30,42] This suggested that dye degradation presumably followed a surface-controlled phenomenon wherein the rate-limiting step was essentially a surface–chemical reaction instead of diffusion.

To sum up, combined with the above discussed TEM and IR analyses, the excellent catalytic performance of Fe NPs could be attributed to the following reasons: firstly, these polyphenol-based biomolecules from bael extract afford good dispersion
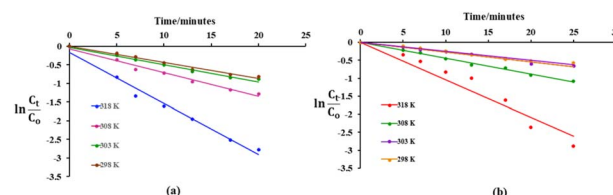

Fig. 5 Plot of removal efficiency (R.E%) *versus* time at different temperatures for (a) reaction conditions: [45 mL of Eosin Yellow dye solution, (8 mg L^{-1}), 5.0 mL aqueous H$_2$O$_2$ (30%) solution (0.2 mol), Fe NPs (50 mg), pH = 6, λ_{max} = 518 nm] and (b) reaction conditions: [45 mL of Fuchsin basic dye (4 mg L^{-1}), 5.0 mL aqueous H$_2$O$_2$ (30%) solution (0.2 mol), Fe NPs (50 mg), pH = 6, λ_{max} = 542 nm, reaction type: Fenton].

Fig. 6 Plot of $\ln(C_t/C_0)$ *versus* time for oxidative degradation (a) reaction conditions: [45 mL of Eosin yellow dye solution, (8 mg L^{-1}), 5.0 mL aqueous H$_2$O$_2$ (30%) solution (0.163 mol), Fe NPs (50 mg), pH = 6, λ_{max} = 518 nm] and (b) reaction conditions: [45 mL of Fuchsin basic dye (4 mg L^{-1}), 5.0 mL aqueous H$_2$O$_2$ (30%) solution (0.163 mol), Fe NPs (50 mg), pH = 6, λ_{max} = 542 nm, reaction type: Fenton].

Table 1 Summary of k_{obs} and R^2 values for dye degradation

| Temperature (K)	Eosin yellow		Fuchsin basic	
	k_{obs} (min^{-1})	R^2	k_{obs} (min^{-1})	R^2
298	0.0435	0.9955	0.0253	0.9959
303	0.0486	0.9964	0.027	0.9958
308	0.0691	0.9926	0.0443	0.9976
318	0.1508	0.9953	0.1045	0.9768

and stability to Fe NPs, subsequently effectively improving adsorption of the dye on the surface of these particles. Secondly, the iron nanoparticles reveal small size-distribution, suggesting large specific surface area and availability of more active sites for the Fe NPs.

Reusability is one of the essential attributes for assessing the properties of a catalyst. Henceforth, the fate of the Fe NPs for the Fenton-like oxidation reaction was examined at 318 K by recovering, washing, drying and further subjecting it to multiple runs. Interestingly, the removal efficiency values after the first and third cycle did not show much variation, and only a slight decrease in catalytic activity of reused nanoparticles was observed (Table 2), suggesting that the nano-catalyst showed good reusability up to three runs (Fig. S2, ESI†). Furthermore, the FT-IR spectrum, EDX spectrum and XRD results supported that the structures of the oxides of iron remained intact even after reusing the nanoparticles in dye degradation (Fig. S3, ESI†). However, a slight decrease in the catalytic activity could presumably be due to the deactivation of catalytic sites.

Besides performing the reusability studies, efforts were also directed towards investigating the presence of iron in the degraded solution through AAS to negate the absence of leaching which will otherwise result in metal contamination. Though iron is moderately toxic in comparison to other transition metals, toxic doses of iron and its compounds can lead to serious problems, including depression, rapid and shallow respiration, coma, convulsions and cardiac arrest. Henceforth, appropriate knowledge of the iron content is highly desirable. Thus, considering the interest in using synthesized Fe NPs for a suitable application, their stability against leaching of iron in aqueous solution was tested by performing the model reaction. These degraded dye solutions were run on an atomic absorption spectrophotometer taking distilled water as the blank. The blank sample was reported to have 115 ppb of iron. It was observed that the degraded dye solution had an iron concentration in the range of 125–130 ppb. However, the permissible limit of Fe is 300 ppb (US EPA. Secondary Drinking Water Standards: Guidance for Nuisance Chemicals). Hence it clearly
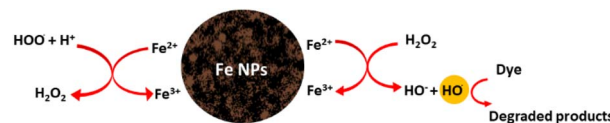
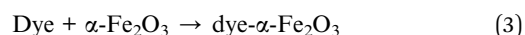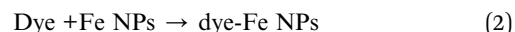**Scheme 1** A schematic representation of the proposed mechanism for oxidative degradation of dyes.

shows that there is negligible leaching of iron from the nanoparticles into the dye solution. This further proves that the use of iron nanoparticles for degrading the dye solution is an environmentally safe method.

Mechanism

On the basis of various experimental results and previous literature reports, a plausible Fenton-like mechanism has been proposed which is in agreement with the mechanism reported by Kuang et al. and Lv et al.[30,43] The oxidative degradation process primarily involves the initial adsorption of the dyes on the surface of the nanocatalyst which is subsequently followed by the surface oxidation reactions. A schematic representation of the proposed mechanism is shown in Scheme 1. First, adsorption of dye onto the surface of Fe NPs occurs (eqn (2) and (3)). Afterwards, Fe(II) and Fe(III) ions leach from Fe(0) and iron oxides on the surface of Fe NPs, as suggested in eqn (4) and (5). At this stage, the decomposition of H_2O_2 is accelerated, forming highly oxidative hydroxyl radicals during Fenton's reaction (eqn (6)). In the meantime, Fe(II) and Fe(III) so released in the solution react with H_2O forming oxyhydroxide (eqn (7)), which can also adsorb dyes. Moreover, surface Fe(III) are converted into Fe(II) and generate HOO$^{\bullet}$ radicals (eqn (8)). Presumably, HOO$^{\bullet}$ radicals so formed further combine with Fe(III) and promote the decomposition of H_2O_2 (eqn (9) and (12)). The highly oxidising hydroxyl radicals rapidly react with the adsorbed dye molecule by breaking the conjugated system in the dye's molecular structure (eqn (13)).[33]
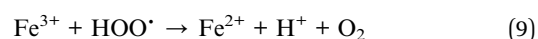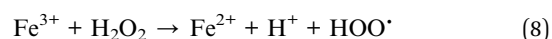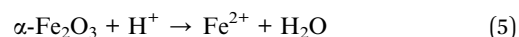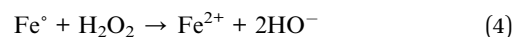
The proposed mechanism for the oxidative degradation of Fuchsin basic dye can be summarised as follows:

(a) Adsorption process

$$\text{Dye} + \text{Fe NPs} \rightarrow \text{dye-Fe NPs} \quad (2)$$

$$\text{Dye} + \alpha\text{-Fe}_2\text{O}_3 \rightarrow \text{dye-}\alpha\text{-Fe}_2\text{O}_3 \quad (3)$$

(b) Degradation on the surface
The process of generation of hydroxyl radicals

$$\text{Fe}^{\circ} + \text{H}_2\text{O}_2 \rightarrow \text{Fe}^{2+} + 2\text{HO}^- \quad (4)$$

$$\alpha\text{-Fe}_2\text{O}_3 + \text{H}^+ \rightarrow \text{Fe}^{2+} + \text{H}_2\text{O} \quad (5)$$

$$\text{Fe}^{2+} + \text{H}_2\text{O}_2 \rightarrow \text{Fe}^{3+} + \text{HO}^- + \text{HO}^{\bullet} \quad (6)$$

$$\text{Fe}^{3+}/\text{Fe}^{2+} + \text{H}_2\text{O}_2 \rightarrow \text{FeOOH} \quad (7)$$

$$\text{Fe}^{3+} + \text{H}_2\text{O}_2 \rightarrow \text{Fe}^{2+} + \text{H}^+ + \text{HOO}^{\bullet} \quad (8)$$

$$\text{Fe}^{3+} + \text{HOO}^{\bullet} \rightarrow \text{Fe}^{2+} + \text{H}^+ + \text{O}_2 \quad (9)$$

Table 2 Variation in efficiency of fresh and reused Fe NPs

Dye	1st cycle	2nd cycle	3rd cycle
Eosin Yellow	97%	90%	85%
Fuchsin Basic	95%	88%	79%

$$Fe^{2+} + HO^\bullet \rightarrow Fe^{3+} + HO^- \tag{10}$$

$$HO^\bullet + HO^\bullet \rightarrow H_2O_2 \tag{11}$$

$$HO^\bullet + H_2O_2 \rightarrow H_2O + HOO^\bullet \tag{12}$$
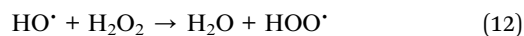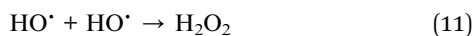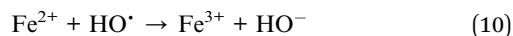
(c) Attack of hydroxyl radicals on the adsorbed dye

$$FB/Fe\ NPs + HO^\bullet \rightarrow reaction\ intermediates/Fe\ NPs \tag{13}$$
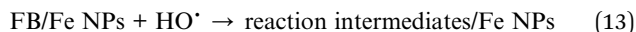
Comparison with literature precedents

As apparent from the comparison in Table 3, *Aegle marmelos* extract has been utilized for the preparation of various iron based catalysts (particularly pristine and doped Fe NPs, entries 1, 2 and 3) and subsequently other plant extract based NPs such as those from *Artocarpus heterophyllus* peel extract (entry 5) which have also been utilized for the degradation of various contaminants. As compared to the previously reported nanoparticles obtained from *Aegle marmelos* extract, the present catalyst offers promising results not just in terms of very high degradation efficiency (>95% within a shorter time duration), but also shows bright prospects of reusability, negligible leaching, *etc.* which are very important parameters to be taken into account in terms of real time industrial applicability. Also, additionally, in comparison to the photo-Fenton conditions reported for the degradation of Eosin yellow dye (entry 4), it can be seen that the degradation efficiency accomplished in the case of the Fenton reaction (present work) is higher than that of the photo-Fenton reaction when iron based catalysts are used.

Besides, a comparative analysis of iron nanoparticles obtained from *Artocarpus heterophyllus* peel extract and *Aegle marmelos* peel extract utilized for the degradation of Fuschin basic also revealed a higher degradation efficiency in case of the latter than the former which evidently highlights the supremacy of the present work (entries 5 and 7).

Experimental procedure

Materials and chemicals

The chemicals employed in the present work were all of analytical grade and used without further purification. FeCl$_2$·6H$_2$O (99.5%), NaOH (98%), and Eosin Yellow (EY) and Fuchsin Basic (FB) dyes were procured from Sigma Aldrich. Stock solutions of the dye were prepared in volumetric flasks by dissolving 8 mg L^{-1} of Eosin Yellow and 4 mg L^{-1} of Fuchsin Basic in distilled water in each case. The varying concentrations of dyes were prepared by diluting the stock solution to the desired concentration with double-deionized water, and thereafter, calibration curves were plotted.

Preparation of bael peel extract

At the outset, the bael peels were washed repeatedly with distilled water to ensure the removal of fine dust particles. Furthermore, before using the peels, they were dried first under

Table 3 Comparison of various iron based catalysts utilized subsequently for degradation of contaminants

Catalyst	Dye	Degradation efficiency	Kinetics studies	Reusability	Ref.
1. Fe doped TiO$_2$ nanoparticles using *Aegle marmelos* leaf extract (photo-Fenton)	Rhodamine B	64% in 60 min using a xenon lamp (500 W) fitted with a 420 nm cutoff filter	—	Not evaluated	46
2. Iron oxide nanoparticles (IONPs) (photo-Fenton)	Brilliant green dye	95.89% in 90 min (under UV light)	First order kinetics model (K value 0.0458 min^{-1})	Not evaluated	47
3. Iron oxide NPs	Not evaluated the catalytic activity for degradation of contaminants	—	—	—	48
4. Fe$_2$O$_3$ NPs (photo-Fenton)	Eosin Yellow	Nearly 90% in 30 min under visible lamp irradiation (high-pressure mercury lamp, 125 watts)	Pseudo first order kinetics (K = 0.08 min^{-1})	Multiple times	49
5. Iron nanoparticles using *Artocarpus heterophyllus* peel extract (Fenton)	Fuchsin Basic	87.5% in the initial 20 mins at 318 K	Pseudo first order kinetics (K = 0.1043 min^{-1})	—	50
6. Iron NPs *Aegle marmelos* peel extract (Fenton)	Eosin Yellow	97% at 318 K within 25 min	Pseudo first order model activation (K = 0.0435 min^{-1})	Up to the third cycle without any noticeable loss in its activity	Present work
7. Iron NPs using *Aegle marmelos* peel extract (Fenton)	Fuschin Basic cationic dye (Fuchsin Basic, FB)	95% at 318 K within 25 min	Pseudo first order model activation (K = 0.0253 min^{-1})	Up to the third cycle without any noticeable loss in its activity	Present work

sunlight for 2–3 days and thereafter placed in a vacuum oven for 2–3 hours, maintaining the temperature at at 60–65 °C. The peels were then ground to a fine powder with the help of a mortar and pestle. To prepare the aqueous extract of the well dried and ground peels, 60 g of the peel powder was taken in a beaker to which 1 L of distilled water was added, and the resulting solution was subjected to stirring at 60 °C until a notable pale yellow coloured aqueous extract solution could be observed.

Preparation of Fe NPs using bael peel extract

To the obtained bael peel extract, 0.1 M FeCl$_2$ solution was added at room temperature, following which NaOH solution was added slowly to adjust the pH of the solution to 6.0. Formation of Fe NPs occurred which could be observed from the colour change of the solution from yellow to intense black. The change in colour is a result of interaction between the polyphenols and ferrous ions, followed by spontaneous reduction of metal ions as suggested by Wang et al.[45] Thereafter, the obtained solution was dried well in an oven, maintaining the temperature between 60 and 80 °C. Formation of a black crystalline precipitate could be observed which was finally ground to a fine powder using a mortar and pestle, washed with ethanol several times and finally dried.

Details of the characterization techniques employed

To validate their identity, various instrumental characterization tools such as FT-IR, SEM/EDX, TEM and XRD techniques were employed. FT-IR of nanoparticles was carried out using the KBr pellet method in a PerkinElmer spectrum 2000 in the range of 400–4000 cm^{-1}. To acquire deep insights into the morphology of the obtained nano-particles, SEM analysis was performed using a JEOL, USA instrument, keeping fixed the electron beam energy of 30 kV at a working distance of 11 mm. Prior to the analysis, the sample was dispersed in ethanol under ultra-sonication and coated with a (10–15) nm layer of high purity gold prior to analysis. Furthermore, for the elemental analysis, EDX (energy dispersive X-ray) analysis was performed using an EDX spectrometer equipped with a SEM instrument with a spectrum acquisition time of 100 s. A TECNAI G2 T30, U TWIN instrument was used for recording TEM images wherein a tungsten or LaB$_6$ filament was used as the electron source. The sample was prepared by dispersing the nanoparticles in ethanol using an ultrasonicator, followed by diluting it well before placing on the Cu grids. Powder X-ray diffraction peaks were obtained with the help of a Bruker D8-Advance Eco powder X-ray diffractometer with Cu-Kα radiation (λ = 1.54056 Å) and a 2θ range of 10–80° at 30 kV and 40 mA. For evaluation of the concentration of Fe(II) ions in the degraded dye solution, a AA-6300 atomic absorption spectrophotometer (Shimadzu Scientific Instruments) was used.

Oxidative degradation experiment

The oxidative degradation experiment was initiated by adding Fe NPs (50 mg) to a 45 mL dye solution in a round bottomed flask, following which 5.0 mL aqueous H$_2$O$_2$ (30%) solution (0.1631 mol) was added, and the resulting suspension was subjected to stirring at room temperature. For monitoring the progress of the reaction, a UV-vis spectrophotometer (λ$_{max}$ = 518 nm for Eosin Yellow; 542 nm for Fuchsin Basic) was employed.

Calibration curves were used for estimating the concentration of the dyes and the removal efficiency was calculated using the following equation:

$$removal\ efficiency\ (R.E\%) = \frac{C_0 - C_t}{C_0} \times 100\% \quad (14)$$

where C_0 (mg L^{-1}) and C_t (mg L^{-1}) represent the initial and the final concentration of the dye solution at t min, respectively. The colour of the dye solutions gradually gets lightened, indicating their degradation Furthermore, to validate the scope of Fe NPs as a true Fenton-like catalyst, a controlled experiment was conducted under similar conditions, without adding Fe NPs, which was also later on used to evaluate the oxidation capability of H$_2$O$_2$ alone in dye degradation.

Recycling and reusability of nanoparticles

Since the constituent of these nanoparticles is a metal, disposing them after use might create environmental problems. However, if these nanoparticles can be recycled and reused, it will be environment friendly. Hence, to understand whether the composition of nanoparticles remains intact or not after use, techniques like FT-IR, SEM-EDX and XRD were also used to analyse the used nanoparticles. After completion of the reaction, the Fe NPs were collected via centrifugation, washed thoroughly with distilled water and ethanol a few times and finally dried. These nanoparticles were then reused to degrade the dye using the same procedure.

Conclusions

This study discloses a green and single-step synthesis of iron nanoparticles using waste bael (Aegle marmelos) peel extract that served as an excellent source of reduction as well as capping agents. TEM analysis demonstrated that nanoparticles exhibited spherical nanostructures with an average crystallite size of around 44 nm. Furthermore, the efficacy of these nanoparticles as a heterogeneous Fenton-like catalyst for dye degradation was also evaluated. The results were encouraging with the nanoparticles displaying catalytic degradation of Eosin Yellow and Fuchsin Basic with a removal efficiency as high as 97% and 95% within 20 and 25 minutes, respectively, at 318 K. The degradation followed pseudo-first order kinetics. The extrapolation of activation energy values of 51.05 and 59.03 kJ mol^{-1}, respectively, suggested that the dye degradation followed a surface-controlled phenomenon. Additionally, the nanoparticles exhibited good reusability and retained catalytic activity as high as 85% up to the third cycle. Atomic absorption spectroscopy analysis revealed that the catalytic system was very stable with negligible leaching of iron from nanoparticles into the dye

solution. Conclusively, the present work offers a sustainable approach that effectively utilizes the waste to develop a heterogenous catalyst, potentially useful for environmental remediation.

Author contributions

All the authors were involved in designing, conceptualization, and experimental and writing work.

Conflicts of interest

There are no conflicts to declare.

Acknowledgements

Notes and references

1 B. I. Kharisov, H. V. Rasika Dias, O. V. Kharissova, V. M. Jiménez-Pérez, B. O. Pérez and B. M. Flores, *RSC Adv.*, 2012, **2**, 9325–9358.

2 D. L. Tejedor, R. Benavent and J. M. Palomo, *Catal. Sci. Technol.*, 2018, **8**, 1754–1776.

3 S. Laurent, D. Forge, M. Port, A. Roch, C. Robic, L. V. Elst and R. N. Muller, *Chem. Rev.*, 2008, **108**, 2064–2110.

4 A. V. Nikam, B. L. V. Prasad and A. A. Kulkarni, *CrystEngComm*, 2018, **20**, 5091–5107.

5 M. Devi, S. Devi, V. Sharma, N. Rana, R. K. Bhatia and A. K. Bhatt, *J. Tradit. Complementary Med.*, 2020, **10**, 158–165.

6 B. Yuliarto, N. L. W. Septiani, Y. V. Kaneti, M. Iqbal, G. Gumilar, M. Kim, J. Na, K. C. W. Wu and Y. Yamauchi, *New J. Chem.*, 2019, **43**, 15846–15856.

7 S. Basak, S. Sikdar, S. Ali, M. Mondal, D. Roy, V. K. Dakua and M. N. Roy, *New J. Chem.*, 2022, **46**, 18055–18068.

8 U. T. P. Nguyen, D. X. M. Bui, T. T. T. Nguyen, N. H. Nguyen, D. T. C. Nguyen and T. V. Tran, *J. Chem. Technol. Biotechnol.*, 2022, DOI: 10.1002/jctb.7305.

9 A. Koutsioukis, G. Florakis, N. Samartzis, S. N. Yannopoulos, M. Stavrou, D. Theodoropoulou and V. Georgakilas, *J. Mater. Chem. C*, 2023, **11**, 3244–3251.

10 D. K. Sarkar, V. Selvanathan, M. Mottakin, A. M. Hasan, M. A. Islam, H. Almohamadi and M. Akhtaruzzaman, *RSC Adv.*, 2023, **13**, 19130–19139.

11 S. Kohli, G. Rathee, S. Hooda and R. Chandra, *RSC Adv.*, 2023, **13**, 1923–1932.

12 L. Huang, X. Weng, Z. Chen, M. Megharaj and R. Naidu, *Spectrochim. Acta, Part A*, 2014, **130**, 295–301.

13 S. Saif, A. Tahir and Y. Chen, *Nanomaterials*, 2016, **6**, 1–26.

14 A. Rao, A. Bankar, A. R. Kumar, S. Gosavi and S. Zinjarde, *J. Contam. Hydrol.*, 2013, **146**, 63–73.

15 S. O. Aisida, N. Madubuonu, M. H. Alnasir, I. Ahmad, S. Botha, M. Maaza and F. I. Ezema, *Appl. Nanosci.*, 2020, **10**, 305–315.

16 S. Kuppusamy, P. Thavamani, M. Megharaj and R. Naidu, *Environ. Technol. Innovation*, 2015, **4**, 17–28.

17 P. P. Gan, S. H. Ng, Y. Huang and F. Y. S. Li, *Bioresour. Technol.*, 2012, **113**, 132–135.

18 N. Basavegowda and Y. R. Lee, *Mater. Lett.*, 2013, **109**, 31–33.

19 S. M. Roopan, R. G. Madhumitha, A. Rahuman, C. Kamaraj, A. Bharathi and T. V. Surendra, *Ind. Crops Prod.*, 2013, **43**, 631–635.

20 S. Venkateswarlu, Y. S. Rao, T. Balaji, B. Prathima and N. V. V. Jyothi, *Mater. Lett.*, 2013, **100**, 241–244.

21 C. Prasad, S. Gangadhara and P. Venkateswarlu, *Appl. Nanosci.*, 2016, **6**, 797–802.

22 R. K. Sharma, S. Yadav, R. Gupta and G. Arora, *J. Chem. Educ.*, 2019, **96**, 3038–3044.

23 K. S. Lin, N. B. Chang and T. D. Chuang, *Sci. Technol. Adv. Mater.*, 2008, **9**, 025015–025024.

24 W. X. Zhang, *J. Nanopart. Res.*, 2003, **5**, 323–332.

25 M. A. Shannon, P. W. Bohn, M. Elimelech, J. G. Georgiadis, B. J. Marinas and A. M. Mayes, *Nature*, 2008, **452**, 301–310.

26 C. Wang, P. Shi, X. Cai, Q. Xu, X. Zhou, X. Zhou, D. Yang, J. Fan, Y. Min, H. Ge and W. Yao, *J. Phys. Chem. C*, 2016, **120**, 336–344.

27 W. L. Wang, Y. Z. Cai, H. Y. Hu, J. Chen, J. Wang, G. Xue and Q. Y. Wu, *Chem. Eng. J.*, 2019, **359**, 168–175.

28 E. Routoula and S. V. Patwardhan, *Environ. Sci. Technol.*, 2020, **54**, 647–664.

29 T. Shahwan, S. A. Sirriah, M. Nairata, E. Boyacı, A. E. Eroğlu, T. B. Scott and K. R. Hallam, *J. Chem. Eng.*, 2011, **172**, 258–266.

30 Y. Kuang, Q. Wang, Z. Chen, M. Megharaj and R. Naidu, *J. Colloid Interface Sci.*, 2013, **410**, 67–73.

31 Y. Wu, S. Zeng, F. Wang, M. Megharaj, R. Naidu and Z. Chen, *Sep. Purif. Technol.*, 2015, **154**, 161–167.

32 J. K. Rao and S. Paria, *Mater. Res. Bull.*, 2013, **48**, 628–634.

33 S. Vasantharaj, S. Sathiyavimal, P. Senthilkumar, F. L. Oscar and A. Pugazhendhi, *J. Photochem. Photobiol., B*, 2019, **192**, 74–82.

34 W. J. Yu, P. X. Hou, L. L. Zhang, F. Li, C. Liu and H. M. Cheng, *Chem. Commun.*, 2010, **46**, 8576–8578.

35 D. R. Wilburn and W. A. Bassett, *Am. Mineral.*, 1978, **63**, 591–596.

36 M. S. H. Bhuiyan, M. Y. Miah, S. C. Paul, T. D. Aka, O. Saha, M. M. Rahaman, M. J. I. Sharif, O. Habiba and M. A. Shaduzzaman, *Heliyon*, 2020, **6**, e04603.

37 N. Nazar, I. Bibi Kamal, M. Iqbal, S. K. Nouren Jilani, M. Umair and S. Ata, *Int. J. Biol. Macromol.*, 2018, **106**, 1203–1210.

38 J. Feng and T. T. Lim, *Chemosphere*, 2007, **66**, 1765–1774.

39 M. Yuan, X. Fu, J. Yu, Y. Xu, J. Huang, Q. Li and D. Sun, Green synthesized iron nanoparticles as highly efficient fenton-like catalyst for degradation of dyes, *Chemosphere*, 2020, **261**, 127618.

40 L. Jia, Z. Shen and P. Su, Relationship between reaction rate constants of organic pollutants and their molecular descriptors during Fenton oxidation and *in situ* formed ferric-oxyhydroxides, *J. Environ. Sci.*, 2016, **43**, 257–264.

41 Z. Cheng, B. Yang, Q. Chen, W. Jia and Z. Shen, *Chem. Eng. J.*, 2018, **332**, 351–360.

42 L. Huang, X. Weng, Z. Chen, M. Megharaj and R. Naidu, *Ind. Crops Prod.*, 2013, **51**, 342–347.

43 X. Lv, Y. Ma, Y. Li and Q. Yang, *Water*, 2020, **12**, 1–19.

44 A. N. D. Krupa and V. Raghavan, *Bioinorganic Chemistry and Applications*, 2014, Article ID 949538, DOI: DOI: **10.1155/ 2014/949538**.

45 Z. Wang, *ACS Sustainable Chem. Eng.*, 2013, **1**, 1551–1554.

46 S. Chaudhary, S. P. Goutam, A. K. Yadav and G. Pandey, *Proc. Natl. Acad. Sci., India, Sect. A*, 2023, 1–10.

47 M. Sriramulu, Balaji and S. Sumathi, *J. Inorg. Organomet. Polym. Mater.*, 2021, **31**, 1738–1744.

48 S. Munjal and A. Singh, *J. Drug Delivery Ther.*, 2019, **9**, 334–341.

49 B. Yaou Balarabe, M. N. Illiassou Oumarou, A. S. Koroney, I. Adjama and A. R. Ibrahim Baraze, *J. Nanotechnol.*, 2023, DOI: **10.1155/2023/1292762**.

50 R. Jain, S. Mendiratta, L. Kumar and A. Srivastava, *Curr. Res. Green Sustainable Chem.*, 2021, **4**, 100086.